Benchmarking gyrokinetic simulations in a toroidal flux-tube

Y. Chen,[1] S. E. Parker,[1] W. Wan,[1] and R. Bravenec[2]
[1]*University of Colorado at Boulder, Boulder, Colorado 80309, USA*
[2]*Fourth-State Research, Austin, Texas 78704, USA*

(Received 22 July 2013; accepted 4 September 2013; published online 23 September 2013)

A flux-tube model is implemented in the global turbulence code GEM [Y. Chen and S. E. Parker, J. Comput. Phys. **220**, 839 (2007)] in order to facilitate benchmarking with Eulerian codes. The global GEM assumes the magnetic equilibrium to be completely given. The initial flux-tube implementation simply selects a radial location as the center of the flux-tube and a radial size of the flux-tube, sets all equilibrium quantities (B, ∇B, etc.) to be equal to the values at the center of the flux-tube, and retains only a linear radial profile of the safety factor needed for boundary conditions. This implementation shows disagreement with Eulerian codes in linear simulations. An alternative flux-tube model based on a complete local equilibrium solution of the Grad-Shafranov equation [J. Candy, Plasma Phys. Controlled Fusion **51**, 105009 (2009)] is then implemented. This results in better agreement between Eulerian codes and the particle-in-cell (PIC) method. The PIC algorithm based on the $v_{||}$-formalism [J. Reynders, Ph.D. dissertation, Princeton University, 1992] and the gyrokinetic ion/fluid electron hybrid model with kinetic electron closure [Y. Chan and S. E. Parker, Phys. Plasmas **18**, 055703 (2011)] are also implemented in the flux-tube geometry and compared with the direct method for both the ion temperature gradient driven modes and the kinetic ballooning modes. © *2013 AIP Publishing LLC*. [http://dx.doi.org/10.1063/1.4821982]

I. INTRODUCTION

Algorithms for Particle-in-Cell (PIC) gyrokinetic simulation are typically first proposed and demonstrated in simplified geometry, e.g., a shearless slab, then implemented in toroidal geometry. This is the case for the split-weight/control variate algorithm of the GEM code[1] and the perturbative approach of the GTC code for the electrons.[2] The well-known difficulties with kinetic electrons, namely the constraint on the time step and the accuracy of the Ampere solver at large β (β is the ratio between the thermal pressure and the magnetic pressure),[3,4] all arise from the fast motion of the electrons along the field line and manifest themselves in simplified geometry. Development of the algorithm is facilitated in the slab geometry by directly comparing simulations with the analytical dispersion relation for waves of interest, such as the Ion-Temperature-Gradient (ITG) modes and the shear Alfvén waves. The subsequent implementation in toroidal geometry is usually not followed by benchmarking study with the same rigor, because exact analytical results similar to the shearless slab dispersion relation do not exist in toroidal geometry. Comparing the results from different codes that implement the same physical model is the only viable approach for the purpose of code verification.

For code verification, the so-called flux-tube model is a useful compromise between the need for easy specification of the problem and the need for retaining toroidal geometry. The flux-tube model (also called the local model) can be defined within a global model as follows.[5] A radially global equilibrium is defined by an arbitrary magnetohydrodynamics (MHD) equilibrium with general flux-surface shapes, the general equilibrium safety factor profile $q(r)$, and the density and temperature profiles $n_s(r)$, $T_s(r)$ for each species s. A local problem is defined by selecting a single flux-surface (labeled r_0) and a radial span $\triangle r$, then removing all r-dependence in all the equilibrium quantities such as the equilibrium magnetic field strength $B(r,\theta)$, its gradient $\nabla B(r,\theta)$, $n_s(r)$, $n_s'(r) \equiv dn_S(r)/dr$, etc. Removing the radial dependence in the equilibrium ensures that the turbulence is homogeneous in radius, which is a reasonable assumption if the modes of interest have wavelengths shorter than the equilibrium scale length. The shape of the selected flux-surface can still be general, but the specification of the equilibrium is then reduced to the specification of a short list of dimensionless parameters: R/L_{ns} for the density scale length, R/L_{Ts} for the temperature scale length, $\hat{s} = rq\prime/q$ for the magnetic shear, etc. In practice, the general flux-surface shape is usually further simplified, e.g., by using the $s-\alpha$ model or the Miller model,[6] with associated assumptions in handling the poloidal variations in the equilibrium quantities such as $B(r_0,\theta)$. This situation again causes difficulty in code verification, as the term "$s-\alpha$ model" or "the Miller Model" eventually becomes imprecise as one turns to details of code implementation. Fortunately, a standardization of the local equilibrium used in gyrokinetic simulations has emerged over the years in the work of Miller *et al.*,[6] Waltz and Miller,[7] and Candy.[8] This equilibrium model has been used in the GS2 code[9] and the GYRO code,[10] which greatly facilitates the verification between the two Eulerian codes.[11]

The purpose of this paper is to verify the split-weight/control variate algorithm (the direct method) of GEM with the Eulerian codes, and with two alternative PIC algorithms. We first describe the implementation of the Miller-Waltz-Candy local equilibrium model in the GEM code and to present results of benchmarking GEM with the Eulerian codes. The way an arbitrary global equilibrium is handled in the global GEM is first summarized, followed by a description of an initial flux-tube implementation according to the

general procedure outlined above. Comparison between this flux-tube model and GYRO/GS2 show that while there is an overall reasonable agreement, there is disagreement that cannot be resolved with increasing resolution, especially for high-n modes (n is the toroidal mode number). The flux-tube model based on the exact local equilibrium is then presented, with emphasis on the details where this new model differs from the previous model. Simulation results with this new model are in much better agreement with the Eulerian codes. We then implemented two other PIC algorithms in the flux-tube geometry, namely the first gyrokinetic PIC algorithm based on the $v_{||}$ formalism and a generalized Ohm's law,[3] and the gyrokinetic ion/fluid electron hybrid model with kinetic electron closure.[12] The Reynders' algorithm is inaccurate for the finite-β effects, because the stiffness problem at high β values is still present in the Ohm's law and is not solved by Reynders' original algorithm. However, subsequent research in gyrokinetic PIC algorithms has shed much light on this stiffness problem, and a control variate technique similar to that used in the algorithm based on the $p_{||}$ formalism can be employed to improve the accuracy of Reynders' algorithm. Once this is done the $v_{||}$ formalism serves as an independent tool for verification purposes, even though it is proven to be not as efficient as the $p_{||}$ formalism in terms of requirements on the grid resolution and particle numbers.

The gyrokinetic ion/fluid electron hybrid model with kinetic closure ("the closure scheme") is developed in the context of studying the energetic particle driven Alfvén waves. The hybrid model without kinetic electron closure[13] has been used to study the linear stability of high-n Toroidal Alfvén Eigenmodes (TAE) in a burning plasma[14] and the beam driven Reverse Shear Alfvén Eigenmodes (RSAE) in DIII-D.[15] The numerical property of the hybrid model with the kinetic electron closure has been explored in a shearless slab.[12] It was found that the closure scheme is less efficient than the direct algorithm[16] for ion-Larmor-radius scale drift waves, but is more efficient for long wavelength Alfvén waves. This closure scheme has been implemented in the flux-tube geometry and we find that the previous conclusion holds as well in the toroidal geometry. The closure scheme is efficient for kinetic ballooning modes (KBM), a mode of Alfvénic characteristics, but it is difficult to obtain converged results for the ITG driven modes that agree with the direct method. The agreement between the closure scheme and the direct method on the KBMs is an important verification for both algorithms. This is important because, unlike the $v_{||}$ formalism which is implemented here for the purpose of verification only and is not expected to be used in practical simulations, the closure scheme will be the primary tool for studying low-n MHD waves. It is worth noting that efforts to improve particle-in-cell gyrokinetic simulation algorithms have continued up to the present time (see, e.g., the development of a new double-split-weight scheme for shear Alfvén waves[17]), and the numerical properties of the three PIC algorithms studied in this paper in toroidal geometry might be of more broad interest.

The paper is organized as follows. In Sec. II, the flux-tube model is described and benchmarking results with the Eulerian codes are presented. Section III compares the direct method with the alternative PIC algorithms, and summary is given in Sec. IV.

II. THE LOCAL MODEL

Assuming that turbulence eddies have characteristic scale length much smaller than the equilibrium scale length ($\sim a$, the minor radius), drift wave turbulence can be approximately treated as radially homogeneous and can be studied with the flux-tube simulation model,[5] in which radial variation of the equilibrium, both in the magnetic configuration and in the density/temperature profiles, is not retained. Most of the gyrokinetic codes currently in use have the capability of handling a general equilibrium; however, most validation studies of the gyrokinetic model employ flux-tube simulations. It appears that the validity of the flux-tube model can be directly checked with global simulations, but in fact a straightforward global simulation will result in continual profile relaxation, and steady state turbulence can only be achieved by including physical or numerical particle sources and sinks. At the present time, there is no unambiguous interpretation of global simulation results suitable for comparison with flux-tube simulations. For this reason, a flux-tube capability in a global code should be viewed as an independent physical model, rather than a simplified model that requires less computational resource.

The implementation of general equilibrium in a radially global simulation domain has been described in detail previously.[16] The equilibrium magnetic field in an axisymmetric toroidal plasma is given by

$$\mathbf{B} = \mathbf{B_t} + \mathbf{B_p} = \frac{f(\Psi)}{R}\hat{\zeta} + \nabla\zeta \times \nabla\Psi. \tag{1}$$

Here, $\Psi(R,Z)$ is the poloidal flux function, $f(\Psi)$ is an arbitrary flux function related to the poloidal plasma current, $\mathbf{B_t}$ the toroidal field, $\mathbf{B_p}$ the poloidal field, (R,Z,ζ) are a set of right-handed cylindrical coordinates with R the major radius. These are related to the generalized toroidal coordinates (r,θ,ζ) through a smooth parametrization of the magnetic surface, $R = R(r,\theta)$ and $Z = Z(r,\theta)$, with (r,θ) being the parameters. Here, r is a flux-surface label and can be thought of as half of the horizontal size of the surface at the middle plane, and θ as a poloidal angle. The exact geometrical interpretation of the coordinates (r,θ) depends on the specific form of the parametrization. The field-line-following coordinates (x,y,z) are defined as:

$$x = r - r_0, \tag{2}$$

$$y = \frac{r_0}{q_0}\left(\int_0^\theta \hat{q}(r,\theta)\,d\theta - \zeta\right), \tag{3}$$

$$z = q_0 R_{\mathrm{maj}}\,\theta \tag{4}$$

with ζ being the toroidal angle, r_0 labels the flux surface at the simulation center, and $\hat{q} = \mathbf{B}\cdot\nabla\zeta/\mathbf{B}\cdot\nabla\theta$. The magnetic configuration is completely specified by the functions $f(\Psi)$, the safety factor profile $q(r)$, and the surface shape. The

plasma equilibrium also includes the density and temperature profiles for each species.

To convert a global model into a flux-tube model at a chosen radial location r_0, all the equilibrium quantities are set to their local values at r_0,

$$R(r,\theta) = R(r_0,\theta), \tag{5}$$

$$\mathbf{B}(r,\theta) = \mathbf{B}(r_0,\theta), \tag{6}$$

$$\nabla B(r,\theta) = \nabla B(r_0,\theta), \tag{7}$$

$$\hat{q}(r,\theta) = \hat{q}(r_0,\theta), \tag{8}$$

$$J(r,\theta) = J(r_0,\theta), \tag{9}$$

$$n_e(r,\theta) = n_e(r_0,\theta), \tag{10}$$

$$\kappa_{\rm ne}(r,\theta) = \kappa_{\rm ne}(r_0,\theta), \tag{11}$$

$$\frac{\partial y}{\partial r}(r,\theta) = \frac{\partial y}{\partial r}(r_0,\theta). \tag{12}$$

Here, J is the Jacobian defined through $d^3\mathbf{r} = J dx\, dy\, dz$, $\kappa_{\rm ne}(r) = -d\ln n_e(r)/dr$. Notice that the equilibrium quantities and their derivatives (if needed in the simulation) are separately specified. For instance, the ∇B-drift proportional to $\mathbf{B}\times\nabla B$ is also set to its value at r_0. The quantity $\partial y/\partial r$ appears crucially in the explicit form of the Laplace operator $\nabla_\perp^2$ that appears in both the Ampere's equation and the quasi-neutrality condition.[1]

The only exception to this stipulation is the q-profile. In order to retain the effect of the magnetic shear, it is necessary to retain a linear profile in the flux-tube model. This linear q-profile appears only in the boundary condition that maps a position in y at one end of the flux-tube, $\theta = \pi$, to a position in y at the other end, $\theta = -\pi$, according to the x-coordinate.[5] The boundary condition in x and y at any fixed z is periodic in a flux-tube model, consequently the field equations are most efficiently solved using Fourier transform.

The flux-surface shape at r_0 is still arbitrary in the flux-tube model. For code verification purposes, it is convenient to use a simplified model for the flux-surface. The Miller model[6] specifies the local flux-surface shapes through the elongation profile $\kappa(r)$, the triangularity profile $\delta(r)$, and the Shafranov shift profile $R_0(r)$ that gives the geometric center of the flux-surface. Adopting the Miller model, a flux-tube problem is fully specified by a number of dimensionless parameters, such as R_0/a, r_0/a, $R/L_{\rm ns}$ with $L_{\rm ns}$ being the density scale length for species s, $\beta_e = \mu_0 n_e T_e/B^2$, etc. Below we use the local plasma of DIII-D discharge 128913 at the radius $\rho = 0.5$ (ρ is the square root of the normalized toroidal flux) for benchmarking the flux-tube model of GEM with the Eulerian codes GYRO and GS2. This case is ideal for the verification of GEM because it has been studied extensively[11] and good agreement, in both linear and nonlinear simulations, is already achieved between the Eulerian codes. The parameters for the case are given in Table I of Bravenec[11] and will be omitted here. Below we use linear simulations of a single toroidal mode for benchmarking. In such simulations, the box size in y is chosen to be $L_y = 2\pi r_0/nq_0$ with n being the toroidal mode number. The radial box size is chosen to be the minimal value that satisfies both radial periodicity in x and periodicity in y, $L_x = 1/nq\prime$. A scan over n is performed for each of the following three physical models: shaped flux-surfaces with adiabatic electrons, circular flux-surfaces with kinetic electrons, and shaped flux-surfaces with kinetic electrons. In all simulations, a single ion species (deuterium) is included and there are no collisions. The mode frequency and growth rate for the three models are shown in Figs. 1–3. The GEM results obtained here are indicated as "GEM old." Another set of GEM results indicated as "GEM new" will be explained presently. In the case of adiabatic electrons, GEM results agree with GYRO. When kinetic electrons are added, GEM results disagree with GYRO for high-n modes, particularly in the case of circular flux surfaces.

In trying to resolve this disagreement, we initially focus on possible discrepancy in the forms of the guiding center motion in different codes. The simple form used in GEM[16] is known to be non-Hamiltonian. In the δf-method, the marker particle distribution is assumed to be the initial loaded Maxwellian distribution, uniform in space. It is trivial to show that such a uniform Maxwellian is an exact equilibrium solution of the drift kinetic equation, provided that the guiding center motion is Hamiltonian. A non-Hamiltonian guiding center motion might cause bunching of the markers in a PIC simulation, which requires correction in the particle weight equation. This error, if important, does not appear (or at least figures differently) in an Eulerian code that employs fixed phase-space grids. Thus, our first step in resolving the disagreement is to implement the Hamiltonian form of the guiding center motion.[18] However, this improved guiding center motion makes no difference in the current verification study.

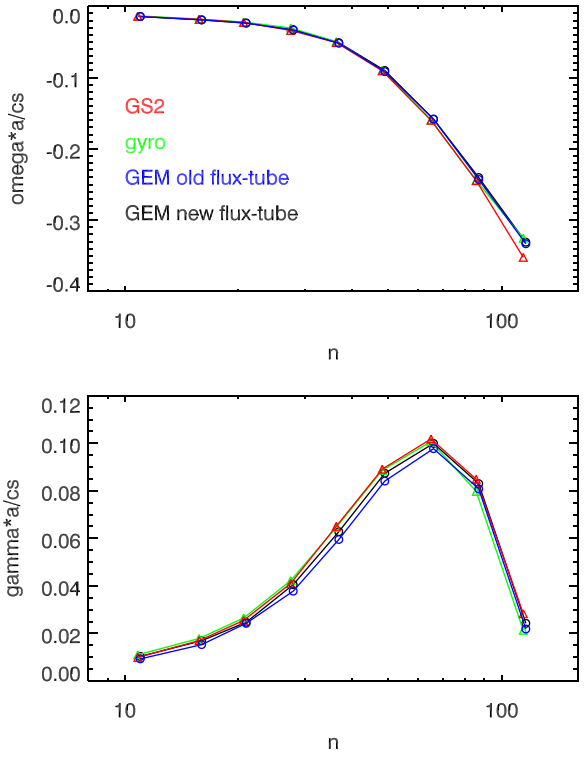

FIG. 1. Mode frequency and growth rate vs. the toroidal mode number, Bravenec Case,[11] with adiabatic electrons.

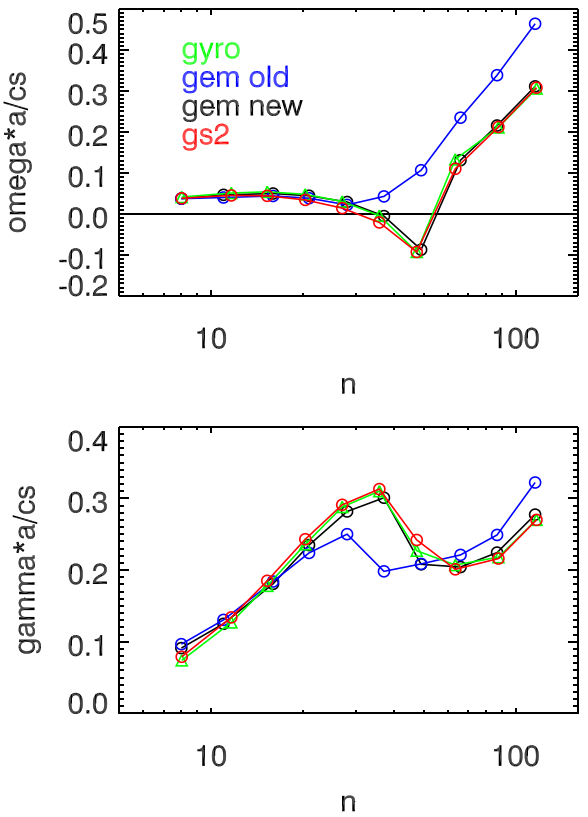

FIG. 2. Mode frequency and growth rate vs. the toroidal mode number, Bravenec Case with kinetic electrons, circular flux surfaces.

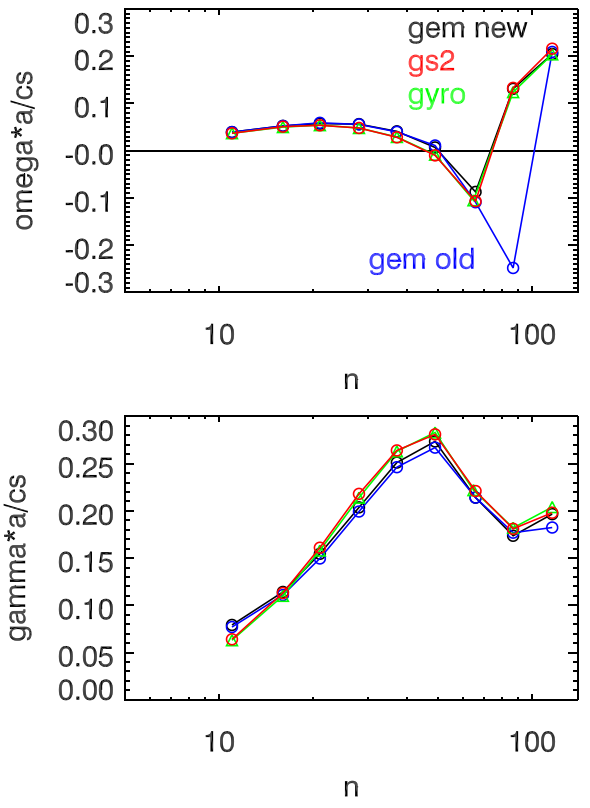

FIG. 3. Mode frequency and growth rate vs. the toroidal mode number, Bravenec Case, shaped flux surfaces.

A. Flux-tube model with exact local equilibrium

The observed disagreement is eventually traced back to the different ways the Miller specification of the flux surface shape is interpreted in GEM and GYRO. A Miller parametrization of the surface shape is given by

$$R = R_0(r) + r\cos(\theta + (\arcsin\delta(r))\sin\theta), \tag{13}$$

$$Z = \kappa(r) r \sin\theta. \tag{14}$$

Locally, the shape is determined by the six parameters: the major radius $R_0(r_0)$ and the Shafranov shift $\triangle \equiv dR_0/dr$, the elongation κ and its radial variation $s_\kappa = r_0 d\ln\kappa/dr$, and the triangularity δ and its radial variation given by $s_\delta \equiv r_0 d\delta/dr$. The flux-tube model described above assumes that the nested flux surfaces near r_0 described by this set of local parameters are indeed part of an exact local solution of the Grad-Shafranov (G-S) equation. This is in general not the case, and here lies the difference between the above flux-tube implementation and GYRO's flux-tube model, which is based on the exact G-S solution of Miller *et al.*[6–8] In the GYRO model, the flux surface at r_0 is still given by $\{R_0, \kappa, \delta\}$, but the three derivatives $\{\triangle, s_\kappa, s_\delta\}$ should not be viewed as determining the nearby surfaces literally as if, e.g., the elongation at $r_0 + dr$ is $\kappa + \kappa' dr$ with $\kappa' = \kappa s_\delta / r_0$. The flux surface shape at $r_0 + dr$ is determined by the G-S equation, and in general is not of the form of Eqs. (13) and (14). The six shaping parameters are used to completely specify the poloidal equilibrium field, which is then used as a boundary condition that completely determines the local G-S solution. If the global equilibrium one starts with to set up the local flux-tube problem is indeed an exact G-S equilibrium, then there is no difference between the two approaches to construct a flux-tube problem, but for a model global equilibrium given by Eqs. (13) and (14), the two flux-tube problems are not equivalent. Details of the flux-tube model based on the local G-S equilibrium can be found in Candy.[8] The required modifications in GEM are summarized as follows. No changes are needed in the poloidal dependence of any equilibrium quantities because at r_0 the flux surface shape is imposed as a boundary condition. The local density and temperature gradients are used as input and do not need reinterpretation. The local variation of the poloidal current profile, $f(\Psi)$ in Eq. (1), is determined in the local equilibrium and has been implemented previously.[1] The radial variation of B is calculated with Eq. (72) of Ref. 8, and the radial variation of the coordinate y, which is up to a constant factor identical to the "eikonal function" of Ref. 8, is calculated with the aid of Eqs. (73) and (81) of Ref. 8.

The results from this new flux-tube model are also shown in Figs. 1–3, in good agreement with the Eulerian codes. The comparison between the Eulerian method and the Lagrangian PIC method here obtained is an improvement over the previous comparison[1,16] as a result of using a standardized equilibrium model.[8] We are expanding this verification studies by, e.g., adding collisions, equilibrium shear flow, and nonlinearity, and will report those new results elsewhere.[19]

III. NUMERICAL STUDY OF THE GYROKINETIC ION/FLUID ELECTRON HYBRID MODEL WITH KINETIC ELECTRON CLOSURE

This section is a continuation of our previous numerical study[12] of the gyrokinetic ion/fluid electron model with kinetic closure (the "closure scheme"). The underlying physical model of this closure scheme is the same gyrokinetic-Maxwell system of equations as that solved by the usual split-weight scheme with a control-variate Ampere solver[1,16] (the "direct method"). For this reason, the closure scheme in its complete form should be viewed as only a new algorithm, but the way it is structured does allow for simple variations that change it into simplified physical models, such as a massless fluid electron model.[20] In fact, the closure scheme originated from the mass-less fluid electron model. The latter was first employed to circumvent numerical difficulties due to kinetic electrons, but in time those difficulties have been directly solved for drift wave turbulence simulations. The fluid electron model, however, has proven to be very efficient for the simulation of low-n energetic particles driven Alfvén waves.[13–15] It is therefore desirable to improve the fluid electron model by including kinetic electron effects through particle closure. The formulation of this closure scheme is described and demonstrated previously in a 3-D shearless slab.[12] The main conclusions of the previous study is: (a) for ion Larmor radius scale drift waves with $k_\perp \rho_i \sim 1$, the direct method is more efficient than the closure scheme; and (b) for long wavelength Alfven waves, the closure scheme is both more accurate and more efficient than the direct method. Our purpose in this section is to implement the closure scheme in a flux-tube and to explore the numerical property of the closure scheme in toroidal geometry. As will be seen, the previous conclusions hold true in toroidal geometry as well, showing that the closure scheme is clearly preferred for energetic particle physics.

The gyrokinetic-Maxwell system of equations includes the ion gyrokinetic equation, the electron drift-kinetic equation, the quasi-neutrality condition, and the Ampere's equation. The electromagnetic field of the hybrid model is given by $\delta \mathbf{B} = \nabla \times (A_{||}\mathbf{b})$ and $\delta \mathbf{E} = -\nabla\phi - (\partial A_{||}/\partial t)\mathbf{b}$, $\mathbf{b}$ is the unit vector along the unperturbed magnetic field. The parallel component of $\delta \mathbf{E} = -\nabla\phi - (\partial A_{||}/\partial t)\mathbf{b}$ is cast into the form

$$\frac{\partial A_{||}}{\partial t} = -\mathbf{b}\cdot\nabla\phi - E_{||}, \tag{15}$$

which is integrated in time to obtain $A_{||}$. The Ampere's equation is then used to calculate the electron parallel flow $u_{||e}$. The parallel electric field $E_{||}$ is given by the Ohm's law,

$$\begin{aligned} en_0 E_{||} - \frac{m_e}{\mu_0 e}(\nabla_{||}\nabla_\perp^2\phi + \nabla_\perp^2 E_{||}) \\ = -\nabla\cdot\int m_e v_{||}\mathbf{v}_G f_{e1}\, d\mathbf{v} - \int \mu\mathbf{b}\cdot\nabla B_0 f_{e1}\, d\mathbf{v} \\ - \int m_e v_{||}^2 \frac{\delta\mathbf{B}_\perp}{B_0}\cdot\nabla f_{0e}\, d\mathbf{v} + \text{ion terms}. \end{aligned} \tag{16}$$

This equation is derived by taking the time derivative of the Ampere's equation and obtaining the rate of change of the parallel electron and ion current by taking the $v_{||}$-moment of the kinetic equations. Here, f_{e1} and f_{e0} are the perturbed and equilibrium electron guiding center distribution, respectively. $\mathbf{v}_G = v_{||}\mathbf{b} + \mathbf{v}_D$ is the guiding center velocity. For simplicity, the ion contributions are not written out explicitly. These ion terms are nominally $\sim m_e/m_i$ smaller than the electron terms, but must be retained for the simulation of ion acoustic waves (IAW)[21] or the ITGs which involve coupling of drift waves and IAWs.[22] They are not needed for Alfvenic waves including the KBM. In a slab geometry, the unperturbed guiding center velocity is $\mathbf{v}_G = v_{||}\mathbf{b}$. If we assume a fixed electron temperature, then the explicit m_e-dependence on the RHS of Eq. (16) drops out upon integration. The only term that depends on the electron mass is the second term on the LHS. As will be see below, the utility of the closure scheme entirely depends on, for the mode of interest, whether this electron inertia term is important in the Ohm's law.

The electron pressure also appears in the continuity equation

$$\begin{aligned} \frac{\partial \delta n_e}{\partial t} + (B\nabla_{||} + \delta\mathbf{B}_\perp\cdot\nabla)\frac{n_e u_{||e}}{B} + \mathbf{v}_E\cdot\nabla n_e \\ + \frac{1}{m_e\Omega_e B^2}\mathbf{B}\times\nabla B\cdot\nabla(\delta p_{\perp e} + \delta p_{||e}) \\ + \frac{2n_0}{B^3}\mathbf{B}\times\nabla B\cdot\nabla\phi = 0, \end{aligned} \tag{17}$$

which is integrated in time to obtain the perturbed electron density δn_e. The kinetic closure scheme for electrons amounts to calculating $\delta p_{||e}$ and $\delta p_{\perp e}$ in Eq. (17), and the electron terms on the RHS of Eq. (16), using the drift-kinetic equation. In a shearless slab geometry, only the parallel pressure $\delta p_{||e}$ in the Ohm's equation (contained in the second term on the RHS of Eq. (16)) is needed.

The electric potential ϕ is usually obtained with the gyrokinetic Poisson equation. We have found that it is advantageous numerically to solve the vorticity equation (the time derivative of the gyrokinetic Poisson equation) for $\dot{\phi} \equiv \partial\phi/\partial t$ and integrate $\dot{\phi}$ to obtain ϕ.[15] This vorticity approach will be adopted in the following simulations.

The Ohm's equation Eq. (16) displays the well-known "cancellation problem" characteristic of problems that involve finite-β effects and kinetic electrons. For a typical experimental plasma, the electron inertia term is orders of magnitude smaller than the first term on the LHS of Eq. (16). The correct discretization of the Ohm's equation follows a procedure similar to the discretization of the Ampere's equation in the direct method,[16] and is described previously in the slab geometry.[12] The first term on the LHS of Eq. (16) is converted to a summation over the electron markers, similar to the electron terms on the RHS. The equation is then solved iteratively. The perturbed electron distribution f_{e1} is obtained with the usual δf particle simulation method. In the direct method, the split-weight scheme, which separates f_{e1} into an explicit adiabatic piece and the rest, is needed for numerical stability.[16] This is not needed anymore.

Once $E_{||}$ is obtained from the Ohm's equation, it is trivial to implement Reynders' algorithm[3] in the same flux-tube

geometry. As in the direct method, the gyrokinetic Poisson equation is solved to obtain ϕ and the Ampere's equation is solved for $A_{||}$. In contrast to the direct method which uses $p_{||} = v_{||} - (e/m_e)A_{||}$ as a velocity coordinate, the Reynders' algorithm uses $v_{||}$ directly and will be referred to as the $v_{||}$-formalism. The cancellation problem and its solution were not known at the time when electromagnetic algorithms were first attempted,[3] consequently the algorithm (without the correct discretization) is limited to very low-β plasmas. Additionally, the constraint on the time step due to the electron parallel motion is not addressed, and a cut-off technique in the electron response, namely setting the weights of those electrons with $|v_{||}| > v_{\text{cut}}$ to the adiabatic value (which is proportional to $e\phi/T_e$ in electrostatic problems), was used for numerical stability. An aggressive cut-off of $v_{\text{cut}} < v_{\text{Te}}$ is sometimes necessary for numerical efficiency.[3] It might be possible to use the split-weight scheme in the $v_{||}$-formalism to enhance the time step; however, this is not pursued in this paper. Although the cancellation problem is unavoidable, the place where it appears in the $v_{||}$-formalism, Eq. (16), involves the second moment of the electron distribution, whereas in the direct method the problem appears in the Ampere's equation that only involves the first order moment. As will be seen below, this difference leads to different requirements on the grid resolution if a certain accuracy is to be achieved. As a practical tool, the $v_{||}$-formalism is simply not competitive with the direct method. Nevertheless, we have implemented it to provide additional verification for the direct method.

To compare the three numerical schemes, we use the Waltz case[23] parameters: $R/a = 3$, $r_0/a = 0.5$, $q_0 = 2$, $\hat{s} = 1$, with a single deuterium ion species with $T_e/T_i = 1$ and $\rho^* = \rho_s/a = 0.0025$. Here, $\rho_s = m_i c_s/eB$ and $c_s = \sqrt{T_e/m_i}$. The density scale length is $R/L_n = 3$ and the temperature scale length is $R/L_T = 9$. The magnetic equilibrium has concentric circular flux surfaces: $\kappa = 1$, $\delta = 0$, $\triangle = s_\kappa = s_\delta = 0$. Linear simulations of the $n = 28$ ($k_\theta \rho_i = 0.28$) mode are performed scanning over the electron beta $\beta_e \equiv 2\mu_0 n_e T_e/B^2$, for each of the three models/algorithms: the direct method, the $v_{||}$-formalism and the closure scheme. The flux-tube model with the exact local G-S solution is used in the following simulations, except a modification on the thermal pressure effect. The local magnetic equilibrium as determined by the G-S equation changes with β_e, and we found that this effect suppresses the kinetic ballooning mode at high beta. Since the closure scheme is developed mainly for the purpose of simulating waves with Alfvénic character (e.g., the Toroidal Alfvén Eigenmodes or the kinetic ballooning modes), we will remove the β_e-dependence of the magnetic equilibrium in the following simulations.

The following simulations are single-n linear simulations. The direct method uses a grid resolution of $(N_x, N_y, N_z) = (32, 32, 96)$, 16 particles per spatial cell per species. The same grid resolution is used in the closure scheme, but with an increased particle number of 128 per cell per species. A grid resolution of $(N_x, N_y, N_z) = (32, 32, 192)$ is used in the $v_{||}$-formalism simulations with a particle number of 32 per cell per species. The number of grid points along the field line, N_z, is larger than typically used in order to compare only reasonably converged results. The results are shown in Fig. 4. It is difficult to obtain converged results from the closure scheme on the ITG branch, hence only data from the direct method and the $v_{||}$-formalism are shown for the ITGs. The results from the $v_{||}$-formalism agree very well with that of the direct method, for both branches of modes. For the KBMs, the fluid electron model is used both with and without the electron closure. Without the kinetic closure, the fluid electron model becomes the massless fluid electron model with isothermal electrons.[20] As can be seen, the massless fluid model gives a growth rate significantly smaller than the correct results, which here are taken to be the results from the direct method. This is not surprising as it is known that trapped electron effects, missing in the massless fluid model, are important for the ion Larmor radius scale drift waves. Including the kinetic electron closure much improves the accuracy of the fluid electron model. For the KBM branch, the closure scheme results are in good agreement with the direct method.

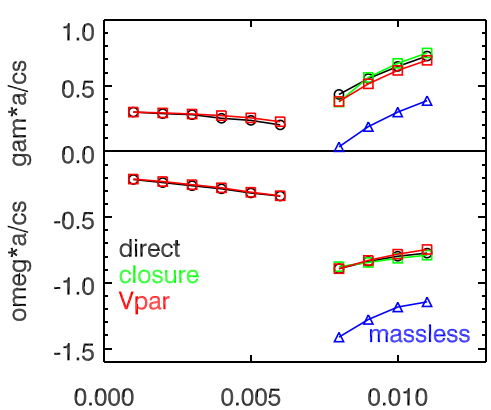

FIG. 4. Mode frequency and growth rate vs. $\beta_e = 2\mu_0 n_e T_e/B^2$, GA Standard Case parameters. The left branch is ITG, the right branch is KBM.

Fig. 5 compares the efficiency of the direct method with that of the $v_{||}$-formalism for the ITG mode, and Fig. 6 compares the efficiency of the direct method with that of the closure scheme for the KBM. Accuracy is most sensitive to the

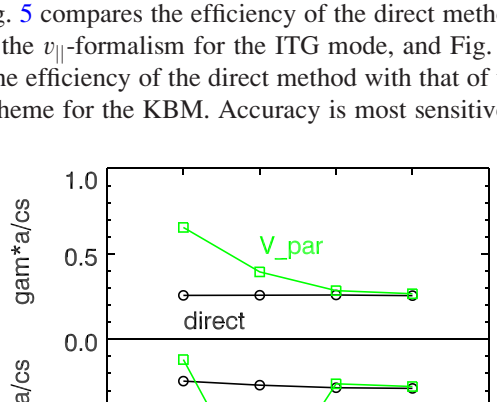

FIG. 5. Convergence rate in the number of grid points along the field line, for the $n = 28$ ITG mode of Figure 4 ($\beta_e = 0.004$), comparing the direct method and the $v_{||}$ formalism.

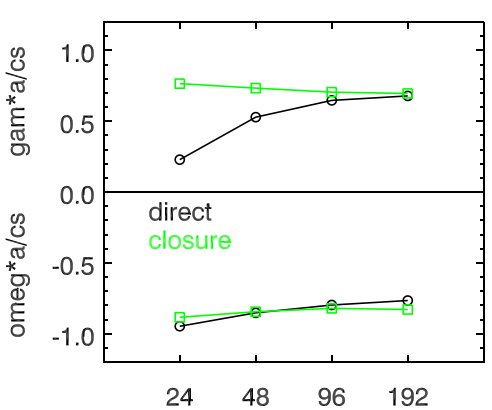

FIG. 6. Convergence rate in the number of grid points along the field line, for the $n=28$ KBM mode of Figure 4 ($\beta_e = 0.01$), comparing the direct method and the closure scheme.

fast streaming of the electrons along the field line. A convergence test in N_z is therefore used to quantify the relative efficiency of a numerical schemes. For the $v_{||}$-formalism results in Fig. 5, 16 particles per species per cell are used; and for the direct method, 8 particles per species per cell. For the closure scheme results in Fig. 6, 32 particles per species per cell are used; and for the direct method, 16 particles per species per cell. Fig. 5 shows that, for ITGs, the direct method converges more rapidly with N_z than the $v_{||}$-formalism. For the KBMs (Fig. 6), both the direct method and the closure scheme converge rapidly with N_z, but the closure scheme is remarkably accurate for moderate N_z (≤ 96).

The good agreement between the direct method and the closure scheme for the KBMs obtained here, and the agreement between the direct method and the $v_{||}$-formalism, are an important case of code verification. What counts as verification is the fact that different codes that solve the same mathematical problem based on different numerical schemes agree on the result. The three schemes studied here, although all use the Particle-in-Cell method, differ sufficiently in algorithmic details. The agreement between them for KBMs establishes the validity of all the algorithms for high-n the Alfvénic waves under consideration. As already mentioned, the $v_{||}$-formalism is not expected to be used in any practical simulations. Based on the results of Fig. 4, one might conclude that the closure scheme is also superfluous, being inaccurate for the ITGs (not shown) and not clearly more efficient than the direct method for the KBMs. The main goal of developing the closure scheme, however, is to add kinetic electron effects in the simulation of energetic particles driven low-n MHD waves. In this regard, it is important to note that, based on previous slab simulations,[12] the closure scheme is both more accurate and robust for low- n Alfven waves than the direct method. We do not expect this conclusion to change in toroidal geometry, but we will leave its direct proof to future work.

The results obtained here concerning the utility of the hybrid model with kinetic closure for the ion-Larmor-radius scale ITG turbulence is negative: the direct method is clearly preferred in terms of numerical efficiency. In this regard, it is worth noting that the GTC code[24] uses a model for the electrons that is similar in appearance to the closure scheme presented here. Both schemes are based on a fluid electron model and both attempt to add kinetic electron effects using PIC simulation. While we expect to use the closure scheme solely for the low-n Alfvénic waves, the GTC scheme is intended to be used for both low-n Alfvénic waves and high-n drift wave turbulence. Does our conclusion concerning the efficiency of the closure scheme bear directly on the GTC scheme? Despite the apparent similarity between the two schemes, significant difference also exists. The closure scheme presented here is exact, whereas the GTC scheme is a perturbative approach, formally being an asymptotic expansion based on the small parameter $\delta = \omega/k_{||}v_{\mathrm{Te}}$. For ITG waves, there are two physical effects associated with the electrons that need to be captured in simulation, namely the trapped electron effects and the finite-β stabilization of the mode. The latter effect is a fluid-effect, as it can be seen in a massless fluid electron simulation.[20] The GTC approach is based on the same fluid electron model as used here, but its perturbative procedure for the electron kinetic effects is specifically constructed to capture the trapped electron effects.[24,25] Hence, it is possible for the perturbative approach to capture both the finite-β effects and the trapped electron effects, while at the same time avoiding solving a cancellation problem. Finite-β modified ITG modes have indeed been seen with GTC.[26] Needless to say, it is desirable to implement the perturbative scheme in the flux-tube geometry and compare it directly with the direct method, but this is beyond the scope of this work.

IV. SUMMARY

In summary, we have implemented the flux-tube model in the GEM code and carried out benchmarking studies between the PIC code and Eulerian codes GYRO and GS2 for linear problems. Good agreement is obtained by implementing in GEM the same magnetic equilibrium as used in the Eulerian codes based on the local solution of the Grad-Shafranov equation. We have also implemented in the flux-tube geometry two other numerical schemes for the same mathematical problem, namely the Reynders' algorithm based on the $v_{||}$-formalism and the gyrokinetic ion/fluid electron model with kinetic electron closure. By comparing results from these alternative schemes with that from the direct method for both the ITG modes and the KBM modes, further verification of the PIC algorithms of GEM is obtained. The feasibility of the kinetically closed hybrid model in terms of accuracy and numerical stability for typical grid resolution and time steps is demonstrated.

ACKNOWLEDGMENTS

This research used resources of the National Energy Research Scientific Computing Center, which is supported by the Office of Science of the U.S. Department of Energy under Contract No. DE-AC02-05CH11231.

[1]Y. Chen and S. E. Parker, J. Comput. Phys. **220**, 839 (2007).
[2]Z. Lin and L. Chen, Phys. Plasmas **8**, 1447 (2001).

[3]J. V. W. Reynders, Ph.D. dissertation, Princeton University, 1992.
[4]J. C. Cummings, Ph.D. dissertation, Princeton University, 1994.
[5]M. A. Beer, S. C. Cowley, and G. W. Hammett, Phys. Plasmas **2**, 2687 (1995).
[6]R. L. Miller, M. S. Chu, J. M. Greene, Y. R. Lin-Liu, and R. E. Waltz, Phys. Plasmas **5**, 973 (1998).
[7]R. Waltz and R. L. Miller, Phys. Plasmas **6**, 4265 (1999).
[8]J. Candy, Plasma Phys. Controlled Fusion **51**, 105009 (2009).
[9]W. Dorland, F. Jenko, M. Kotschenreuther, and B. Rogers, Phys. Rev. Lett. **85**, 5579 (2000).
[10]J. Candy and R. Waltz, J. Comput. Phys. **186**, 545 (2003).
[11]R. V. Bravenec, J. Candy, M. Barnes, and C. Holland, Phys. Plasmas **18**, 122505 (2011).
[12]Y. Chen and S. E. Parker, Phys. Plasmas **18**, 055703 (2011).
[13]J. Lang, Y. Chen, S. E. Parker, and G.-Y. Fu, Phys. Plasmas **16**, 102101 (2009).
[14]Y. Chen, S. E. Parker, J. Lang, and G.-Y. Fu, Phys. Plasmas **17**, 102504 (2010).
[15]Y. Chen, T. Munsat, S. E. Parker, W. W. Heidbrink, M. A. V. Zeeland, B. J. Tobias, and C. W. Domier, Phys. Plasmas **20**, 012109 (2013).
[16]Y. Chen and S. E. Parker, J. Comput. Phys. **189**, 463 (2003).
[17]E. A. Startsev and W. W. Lee, "Finite-beta simulation of microinstabilities," Phys. Plasmas (submitted).
[18]R. G. Littlejohn, J. Plasma Phys. **29**, 111 (1983).
[19]R. V. Bravenec, Y. Chen, J. Candy, S. E. Parker, and W. Wan, "A verification of the gyrokinetic microstability code GEM, GYRO and GS2," Phys. Plasmas (submitted).
[20]Y. Chen and S. E. Parker, Phys. Plasmas **8**, 441 (2001).
[21]Y. Chen and S. E. Parker, Phys. Plasmas **16**, 052305 (2009).
[22]W. Horton, Rev. Mod. Phys. **71**, 735 (1999).
[23]R. E. Waltz, G. Kerbel, and J. Milovich, Phys. Plasmas **1**, 2229 (1994).
[24]I. Holod, W. L. Zhang, Y. Xiao, and Z. Lin, Phys. Plasmas **16**, 122307 (2009).
[25]Z. Lin, Y. Nishimura, Y. Xiao, I. Holod, W. L. Zhang, and L. Chen, Plasma Phys. Controlled Fusion **49**, B163 (2007).
[26]I. Holod and Z. Lin, Phys. Plasmas **20**, 032309 (2013).